EPS95 Ref. **eps0426**
Submitted to: **Pa-2 Pa-14**
Pl-4 Pl-11

EUROPEAN ORGANIZATION FOR NUCLEAR RESEARCH

A Study of Charged P-wave D Meson Production in Semileptonic B Decays

The ALEPH Collaboration

Abstract

A search for the semileptonic decay of B mesons into final states involving charged D^{**} as well as non resonant $D\pi$ is performed in a sample of approximately 3 million hadronic Z decays recorded with the ALEPH detector at LEP. Topological vertex criteria are used to separate the $B \to D^{**}\ell\nu X$ signal from background as well as to search for the non-resonant component $B \to D\pi\ell\nu X$. Preliminary results for the branching fraction into resonant and non-resonant components are presented.

Contribution to the International Europhysics Conference on High Energy Physics
EPS–HEP Brussels, Belgium, 27 Jul.–2 Aug. 1995

1 Introduction

The measured exclusive decays $\overline{\mathrm{B}} \to \mathrm{D}\ell^-\overline{\nu}$ and $\overline{\mathrm{B}} \to \mathrm{D}^*\ell^-\overline{\nu}$ only account for 61±6% [1] of the inclusive branching ratio, contrary to theoretical expectations [2]. Therefore, it is interesting to search for and to measure other exclusive semileptonic decays such as direct four-body decays, $\overline{\mathrm{B}} \to \mathrm{D}^{(*)}\pi\ell^-\overline{\nu}$ or $\overline{\mathrm{B}} \to \mathrm{D}^{**}\ell^-\overline{\nu}$, where D^{**} denotes a generic L=1 (P-wave) charm meson.

Heavy Quark Effective Theory (HQET) predicts four neutral and four charged D^{**} mesons [3], the properties of which are given in Table 1.

			Neutral states			Charged states	
	J^P	J_{lq}	Mass (MeV)	Width (MeV)	Decay Modes	Mass (MeV)	Width (MeV)
D_1^*	1^+	1/2	~ 2420	$\gtrsim 250$	$D^*\pi$	~ 2420	$\gtrsim 250$
D_0^*	0^+	1/2	~ 2360	$\gtrsim 170$	$D\pi$	~ 2360	$\gtrsim 170$
D_1	1^+	3/2	2422±2	19±4	$D^*\pi$	2427±3	29±8
D_2^*	2^+	3/2	2459±2	23±5	$D\pi$, $D^*\pi$	2459±3	21±6

Table 1: Charm mesons with orbital excitations, their quantum numbers, masses, widths, and allowed strong decays into $D\pi$ and $D^*\pi$ in the infinite heavy quark mass limit.

Evidence for the narrow $J_{lq} = 3/2$ states has been established for both neutral [4] and charged [5] mesons through their two body decays. The wide $J_{lq} = 1/2$ states are unobserved and cannot be distinguished from four-body decays with the available statistics. The term *non-resonant* is used in the following sections to label both four-body decays and decays involving the wide D^{**} resonances. Evidence for both neutral and charged narrow D^{**} states in semileptonic B decays has been established by ARGUS [6], OPAL [7] and ALEPH [8].

Given the displaced vertex topology of B decays produced at the Z resonance and the capabilities of the ALEPH detector, a topological search for D^{**} in semileptonic B decays is possible. In a previous analysis [8], the ALEPH collaboration has examined both resonant $\overline{\mathrm{B}} \to \mathrm{D}^{**0}\ell^-\overline{\nu}\mathrm{X}$ and non-resonant $\overline{\mathrm{B}} \to \mathrm{D}^{*+}\pi^-\ell^-\overline{\nu}\mathrm{X}$ semileptonic B decays.

This paper presents a measurement of the decay modes[1] $\overline{\mathrm{B}} \to \mathrm{D}_1^+\ell^-\overline{\nu}\mathrm{X}$, $\overline{\mathrm{B}} \to \mathrm{D}_2^{*+}\ell^-\overline{\nu}\mathrm{X}$, and their non-resonant counterparts. The data sample is 2.94×10^6 hadronic decays of the Z collected with the ALEPH detector at LEP from 1991 to 1994.

The ALEPH detector is described in detail elsewhere [9]. The relevant performance for this analysis is the high precision obtained on the impact parameter resolution (25μm + $95\mu\mathrm{m}/p$, where p is in GeV/c) with the tracking devices [10].

[1] In this paper, charge conjugate reactions are always implied.

2 Semileptonic B Decays into Narrow Resonances

Semileptonic B decays into P-wave charmed mesons have a distinctive 3-vertex topology (see Figure 1).

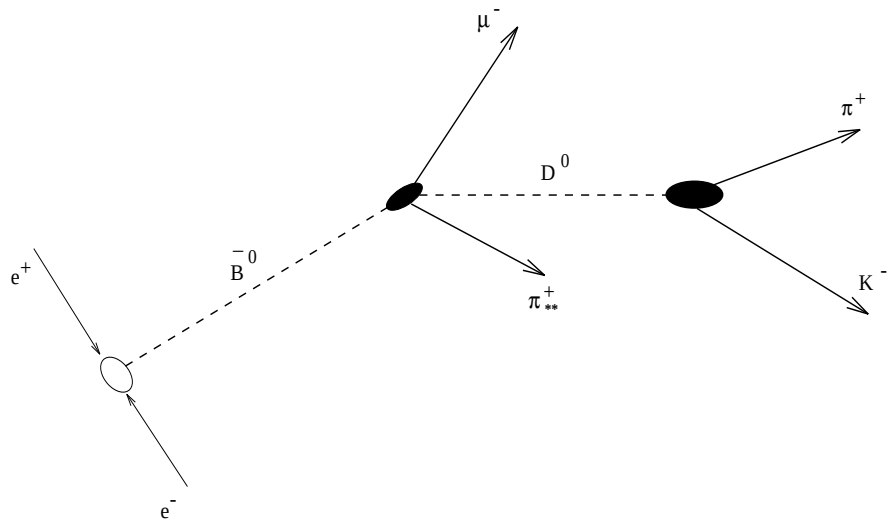

Figure 1: Vertex topology for the decay described in the text.

For the narrow D^{**+} resonance search, the relevant process is the following:

$$\begin{aligned}\overline{B}^0 \longrightarrow\ & D^{**+}\ell^-\overline{\nu} \\ & \hookrightarrow D^0\ \pi^+_{**} \\ & \hookrightarrow D^{*0}\ \pi^+_{**} \\ & \quad\ \hookrightarrow D^0\ (\pi^0 \text{ or } \gamma)\end{aligned}$$

where π^+_{**} denotes the pion from D^{**+} decay. The neutral pion (or photon) from D^{*0} decay is not reconstructed.

The main background to the above signal processes is due to semileptonic B decays into D^0 where the π^+_{**} is a fragmentation track mistakenly associated to the B vertex. This is referred to as *physics background*. The other source of background is due to fake combinations when reconstructing the D^0, which is referred to as *combinatorial background*.

Semileptonic B decays are identified in hadronic events containing a high momentum lepton and a fully reconstructed D^0 meson in the same hemisphere. Lepton identification in ALEPH is described in detail elsewhere [11]. Electron candidates are required to have a momentum greater than 2 GeV/c, muon candidates are required to have a momentum greater than 3 GeV/c.

The D^0 is reconstructed in four decay channels: $D^0 \to K^-\pi^+$, $D^0 \to K^-\pi^+\pi^-\pi^+$, $D^0 \to K^0_S\,\pi^+\pi^-$, and $D^0 \to K^-\pi^+\pi^0$. The mass of the D^0 candidates must lie within $\pm 2\sigma$ of the known D^0 mass, where σ is the standard deviation of the fit to the D^0 mass distribution. To eliminate contamination from D^{*+} decays, other charged tracks (denoted as "π") are paired with the reconstructed D^0: the event is rejected if any combination has a mass difference $|M(D^0\text{"}\pi\text{"}) - M(D^0)|$ less than 5 MeV/c^2 from 145.5 MeV/c^2. The momentum of the D^0 is required to be greater than 5 GeV/c for the $K^-\pi^+$ and $K^-\pi^+\pi^-\pi^+$ decays, 10 GeV/c for the $K^-\pi^+\pi^0$ decay, and 7 GeV/c for the $K^0_S\,\pi^+\pi^-$ decay. The specific ionization measurement, when available, must be consistent with the expected rate for kaons for the $K^-\pi^+\pi^-\pi^+$ and $K^-\pi^+\pi^0$ modes. For these modes, the kaon candidate must have a momentum greater than 1.5 GeV/c. A cut is also made on the track probability to originate from the interaction point [13] in order to reject combinatorial background for the $D^0 \to K^-\pi^+\pi^-\pi^+$ decay. The ρ, K^{*-}, and $\overline{K}^{*0}$ resonances are exploited for the $D^0 \to K^-\pi^+\pi^0$ decay mode. Neutral pions from this decay are identified by fitting pairs of ECAL energy deposits using the constraint that the mass of the pair is consistent with the π^0 mass. For $D^0 \to K^0_S\,\pi^+\pi^-$ we exploit the K^{*-} resonance. K^0_S candidates are rejected if the measured mass is more than 2σ (± 10 MeV/c^2) from the nominal K^0_S mass. Pions from the K^0_S decay are required to be inconsistent with tracks originating from the interaction point.

Reconstructed D^0 mesons and leptons are fitted to a common B vertex using a topological technique. Track candidates are required to have a χ^2 vertex probability greater than 1% for both D^0 and $D^0\ell$ vertices. The $D^0\ell$ vertex is required to be separated by more than three times the resolution of the decay length from the interaction point, and the decay length resolution is required to be less than 500 μm. The $D^0\ell$ vertex is required to be upstream of the D^0 vertex. The invariant mass of the $(D^0\ell)$ candidates is required to be within 2.7 and 5.5 GeV/c^2.

The D^0 candidate mass spectra for the four subsamples are shown in Figure 2. Table 2 summarizes these subsample sizes and background rates from the fits to these distributions.

Pion candidates from D^{**} decays are selected using a momentum cut of 1 GeV/c. True π^+_{**} have a harder momentum spectrum than background fragmentation tracks. This cut

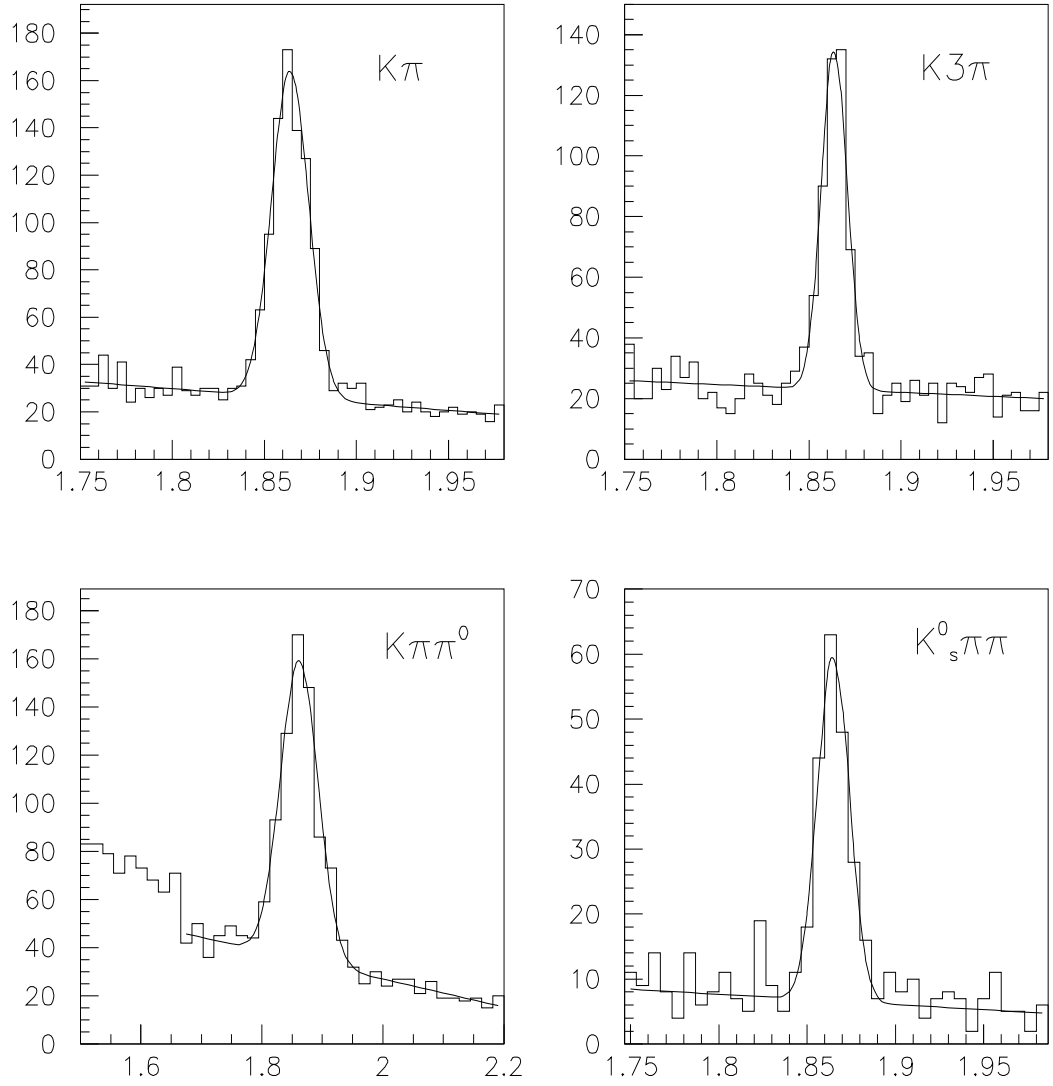

Figure 2: D^0 mass distribution for the decays described in the text.

Channel	D^0 resolution (MeV/c^2)	$D^0\ell$	bkg.
$D^0 \to K^-\pi^+$	10	696±32	207±14
$D^0 \to K^-\pi^+\pi^-\pi^+$	7	396±25	129±11
$D^0 \to K^0_S\,\pi^+\pi^-$	9	180±17	35±6
$D^0 \to K^-\pi^+\pi^0$	31	525±33	235±15

Table 2: D mass resolutions with fitted number of $D\ell$ and background events within a $\pm 2\sigma$ window around the fitted mass.

also reduces uncertainties due to multiple scattering. A π^+_{**} candidate is rejected if its impact parameter with respect to the interaction point is less than twice its uncertainty. The distribution of the impact parameter with respect to the ($D^0\ell$) vertex divided by its uncertainty is used to build a function which gives the probability $\mathcal{P}$ that the π^+_{**} originates from the $D^0\ell$ vertex. This procedure has been decribed in detail in [8] and [12]. Figure 3 shows the $\mathcal{P}$ distribution for simulated signal events; Figure 4 refers to physics background simulated events. The $\mathcal{P}$ probability distribution for signal is expected to be flat, while the $\mathcal{P}$ distribution for background peaks at zero allowing good background rejection. Pion candidates are required to have $\mathcal{P} > 0.1$, which eliminates 80% of the physics background. If more than one $D^0\ell\pi^+_{**}$ combination per event is found, the combination with the greatest probability $\mathcal{P}$ is chosen. This happens for roughly 3%-5% of the events, depending on the channel.

2.1 Results

The parameter Δm^{**} is defined as the difference between the measured masses of the $D^0\pi^+_{**}$ system and the D^0 and has a measurement error of 5 MeV/c^2, which is much less than the natural widths of the D_1^+ and D_2^{*+} resonances. The Δm^{**} distributions are shown in Figure 5 for the right sign sample, the wrong sign sample, and a sample obtained from right sign combinations with a π^+_{**} candidate coming from the interaction point instead of the $D^0\ell$ vertex, referred to as an *anti-tagged vertex sample*. This anti-tagged vertex sample is obtained by reversing the cuts on the impact parameter with respect to the interaction point and on the probability $\mathcal{P}$. There is a significant excess in the right sign sample corresponding to the D_1^+; no excess is found for the D_2^{*+} resonance. The Δm^{**} distribution is fitted with 3 Breit-Wigner functions plus a background function. Two Breit-Wigner account respectively for the D_1^+ and D_2^{*+} decays into $D^{*0}\pi^+$ where the π^0 or γ from the D^{*0} decay is not reconstructed. The third Breit-Wigner accounts for the D_2^{*+} decay into $D^0\pi^+_{**}$. The masses and widths of the Breit-Wigner functions have been fixed according to the D_1^+ and D_2^{*+} known values [1]. The fitted number of events in the D_1^+ signal peak is 32.4±9.4; for the D_2^{*+} resonance, 0.2±7.4 events are fitted. If the masses and widths of the resonances are allowed to vary in the fit, values of 2431±4 MeV/c^2 and

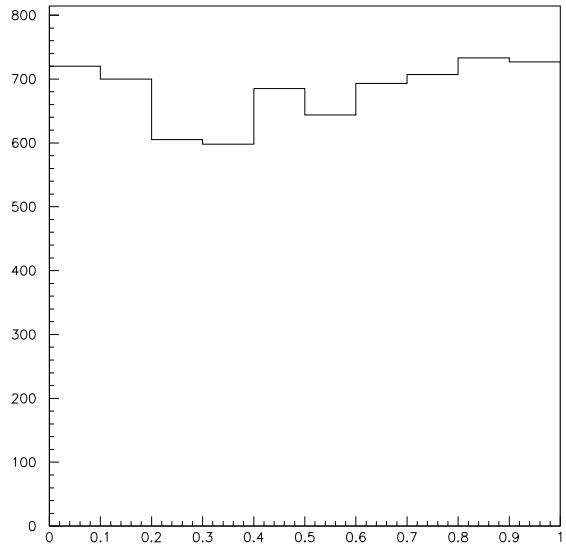

Figure 3: The Probability distribution $\mathcal{P}$ for π^+_{**} to be associated with the Dℓ vertex for simulated signal events.

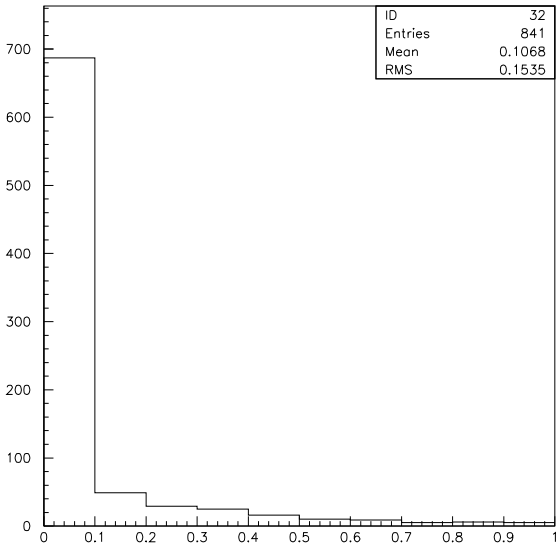

Figure 4: The Probability distribution $\mathcal{P}$ for π^+_{**} to be associated with the Dℓ vertex for simulated physics background events.

19 ± 10 MeV/c^2 are found for the mass and width of the D_1^+ particle, which are consistent within errors with the known values. The product branching ratio for the D_1^+ is:

$$\begin{aligned}\mathrm{Br}(b \to \overline{B}) \times \mathrm{Br}(\overline{B} \to D_1^+ \ell^- \overline{\nu} X) \times \mathrm{Br}(D_1^+ \to D^0 \pi^+) = \\ = (2.06^{+0.58}_{-0.64}(\mathrm{stat})^{+0.30}_{-0.53}(\mathrm{syst})) \times 10^{-3}\end{aligned}$$

The evaluation of systematic uncertainties is given in the next section.

A limit can be set on the production of D_2^{*+}. This is done by refitting the distribution excluding the region within ±2 half-widths of the D_2^{*+} Breit-Wigner. This fit has been used to estimate the background to any possible D_2^{*+} contribution. At 95% confidence level, we obtain:

$$\mathrm{Br}(b \to \overline{B}) \times \mathrm{Br}(\overline{B} \to D_2^{*+} \ell^- \overline{\nu} X) \times \mathrm{Br}(D_2^{*+} \to D^0 \pi^+) \leq 0.77 \times 10^{-3}$$

The D_1^+ product branching ratio agrees with its corresponding isospin conjugate counterpart, as measured in reference [8]. A suppression of D_2^{*+} production relative to D_1^+ production is observed. A similar suppression has been observed in a separate analysis [15].

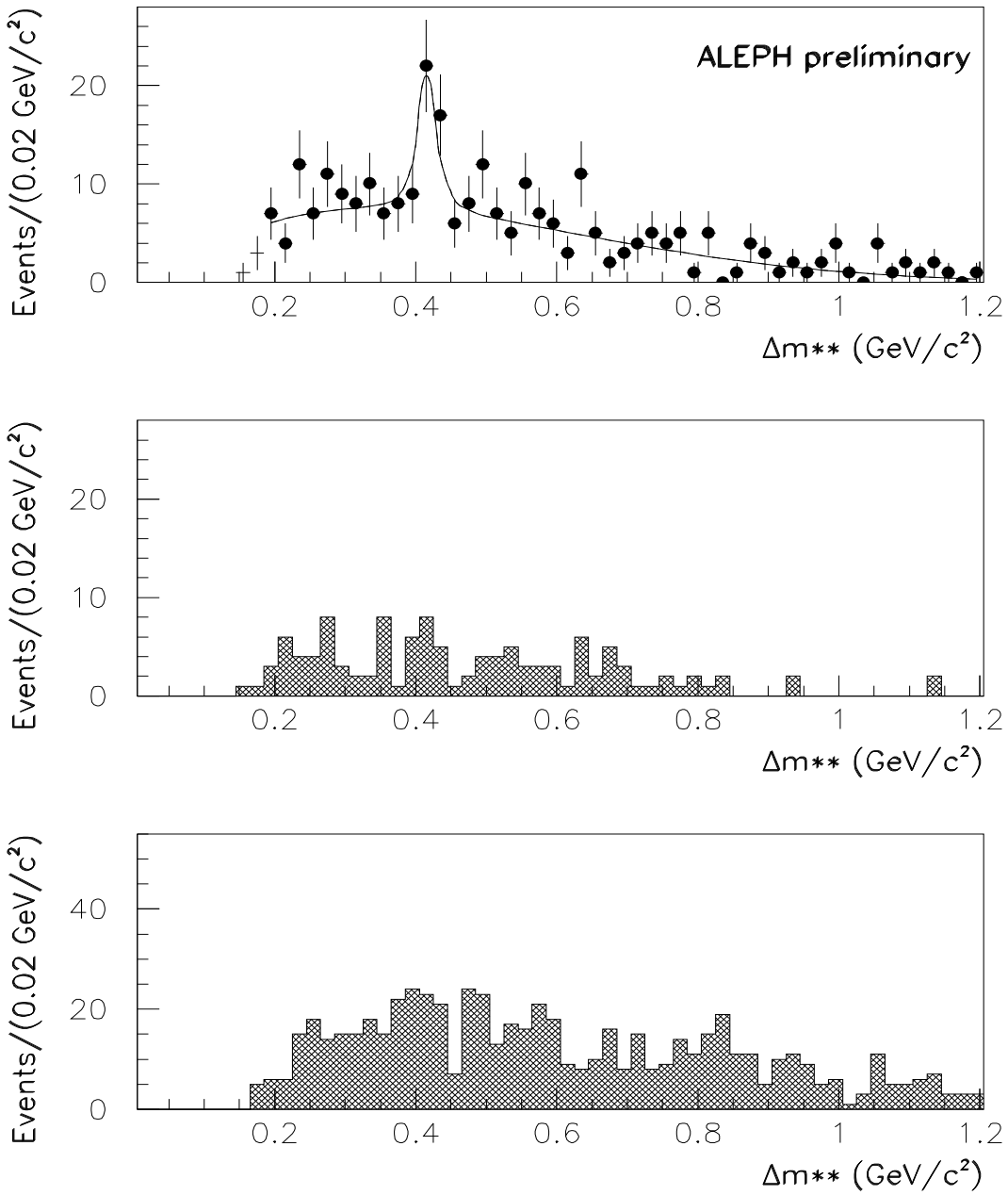

Figure 5: Δm^{**} distributions for the right-sign (top), wrong-sign (middle) and anti-tagged (bottom) samples. Bin width is 20 MeV/c^2.

Channel	$D^0\ell$ Signal Efficiency
$D^0 \to K^-\pi^+$	$7.60 \pm 0.23\%$
$D^0 \to K^-\pi^+\pi^-\pi^+$	$2.44 \pm 0.12\%$
$D^0 \to K^0_S\,\pi^+\pi^-$	$1.52 \pm 0.12\%$
$D^0 \to K^-\pi^+\pi^0$	$0.53 \pm 0.07\%$

Table 3: Efficiencies for $\overline{B} \to D^{**}\ell^-\overline{\nu}$ for the four decay mode. The errors are due to Monte Carlo statistics.

2.2 Systematic Uncertainties

The systematic error due to the uncertainty of D^{**} masses and widths is computed by refitting the distribution varying the masses and widths of the resonances within their published values [1]. The systematic error due to the background parametrization is obtained by fitting with several different background shapes. There is a 10% uncertainty due to the efficiency of the χ^2 requirement for the B vertex. The lepton identification efficiency has an uncertainty of 5%. There is also an uncertainty due to the B fragmentation process which affects the momentum distributions of the decay products. The systematic error due to the B mesons lifetime has been calculated by varying the lifetime within its published uncertainty. An uncertainty due to the shape of the distribution of the distance of the π^+_{**} from the $D^0\ell$ vertex is calculated varying the parameters of the fit to this distribution by their uncertainties.

Systematic uncertainties are summarized in Table 4.

Source	$D^0\ell$ $\sigma_{\rm syst}(10^{-3})$
M,Γ of D^{**}	$^{+0.17}_{-0.47}$
$\Gamma(Z\to b\overline{b})/\Gamma(Z\to had)$	± 0.02
Background Function	± 0.13
B^0 Vertex Efficiency	± 0.13
Monte Carlo Statistics	± 0.06
D^{*+}, D^0 Branching Ratios	± 0.06
Lepton ID Efficiency	± 0.07
b Fragmentation	± 0.11
B^0 Lifetime	± 0.05
Probability Function $\mathcal{P}$	± 0.09
Total	$^{+0.30}_{-0.53}$

Table 4: Systematic uncertainties for $D^0\ell$ for the narrow resonance search.

3 Semileptonic B Decays into Wide and Non-Resonant States

As in the previous analysis, the characteristic topology of the wide $\overline{\mathrm{B}} \to \mathrm{D}^{**+}\ell^-\overline{\nu}$ and non-resonant $\overline{\mathrm{B}} \to \mathrm{D}^0\pi\ell^-\overline{\nu}$ decays permits unambigous identification. Using the $\mathrm{D}^0\ell$ sample selected in the previous section, more stringent requirements are applied to the π^+_{**} candidates. The error on the distance from the $\mathrm{D}^0\ell$ vertex is required to be less than 150 μm, and the impact parameter with respect to the interaction point must be greater than 3 times its uncertainty. If more than one track satisfies these criteria, the candidate with the greatest momentum is chosen.

3.1 Results

The probability distribution $\mathcal{P}$, described in Section 2, is used to estimate the number of signal events. For this search, the π^+_{**} candidates are required to have $\mathcal{P} > 0.2$. The combinatorial background probability shape is taken from $\mathrm{D}^0\ell$ combinations which have an invariant mass in the sidebands of the D^0mass distributions. The corresponding number of events with $\mathcal{P} > 0.2$ is subtracted after correcting for normalization. The number of events from physics background with $\mathcal{P} > 0.2$ is estimated from the fraction of fragmentation pions that fall in the signal region, $f_{\mathcal{P}>0.2}$. From Monte-Carlo simulation $f_{\mathcal{P}>0.2} = 0.125 \pm 0.011$. The probability distributions for the right-sign and wrong-sign samples are plotted in Figures 6 and 7. The excess of right-sign event combinations is evidence of wide- and non-resonant structures. The corresponding $\Delta\mathrm{m}^{**}$ distributions for the right-sign and wrong-sign samples are shown in Figure 8.

The number of signal events in the $\mathcal{P} > 0.2$ region is 70.1±17.0. The corresponding efficiencies are listed in Table 5. The corresponding number of events in the wrong sign combinations is 3±5.

Channel	$\mathrm{D}^0\ell$ Signal Efficiency
$\mathrm{D}^0 \to \mathrm{K}^-\pi^+$	5.00±0.19%
$\mathrm{D}^0 \to \mathrm{K}^-\pi^+\pi^-\pi^+$	1.76±0.11%
$\mathrm{D}^0 \to \mathrm{K}^0_S\,\pi^+\pi^-$	1.13±0.10%
$\mathrm{D}^0 \to \mathrm{K}^-\pi^+\pi^0$	0.413±0.066%

Table 5: Efficiencies for $\overline{\mathrm{B}} \to \mathrm{D}^0\pi\ell^-\overline{\nu}$ for the four decay modes for the non-resonant search.

The branching ratio for the sum of resonant D^{**} and non-resonant contributions is:

$$\mathrm{Br}(\mathrm{b} \to \overline{\mathrm{B}}) \times \mathrm{Br}(\overline{\mathrm{B}} \to \mathrm{D}^0\pi\ell^-\overline{\nu}\mathrm{X}) = (6.46 \pm 1.57(\mathrm{stat}) \pm 0.74(\mathrm{syst})) \times 10^{-3}$$

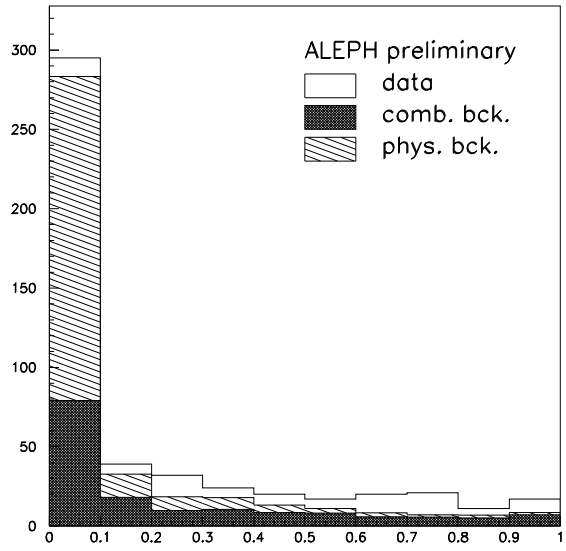

Figure 6: Probability distribution $\mathcal{P}$ for right-sign sample for the non-resonant search. Contributions from combinatorial and physics backgrounds are shown in hatched styles.

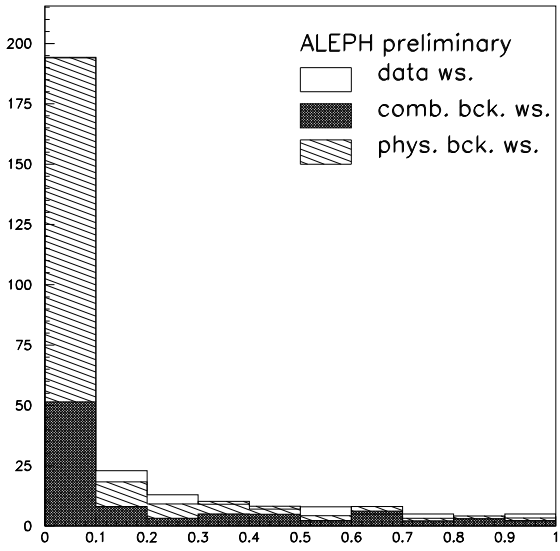

Figure 7: Probability distribution $\mathcal{P}$ for wrong-sign sample for the non-resonant search. Contributions from combinatorial and physics backgrounds are shown in hatched styles.

where the evaluation of systematic uncertainties is given below.

This result is consistent within errors with the corresponding isospin conjugate counterpart as measured in [8]

3.2 Systematic Uncertainties

Systematic uncertainties for the non-resonant analysis are similar to those for the narrow resonant analysis discussed in Section 2.2. A systematic uncertainty of 10% on the efficiency is added since it is not possible to distinguish the contribution due to wide resonant decays from those due to non-resonant decays (the contribution from non-resonant decays is not well known and could have a different efficiency). The systematic uncertainties are given in Table 6.

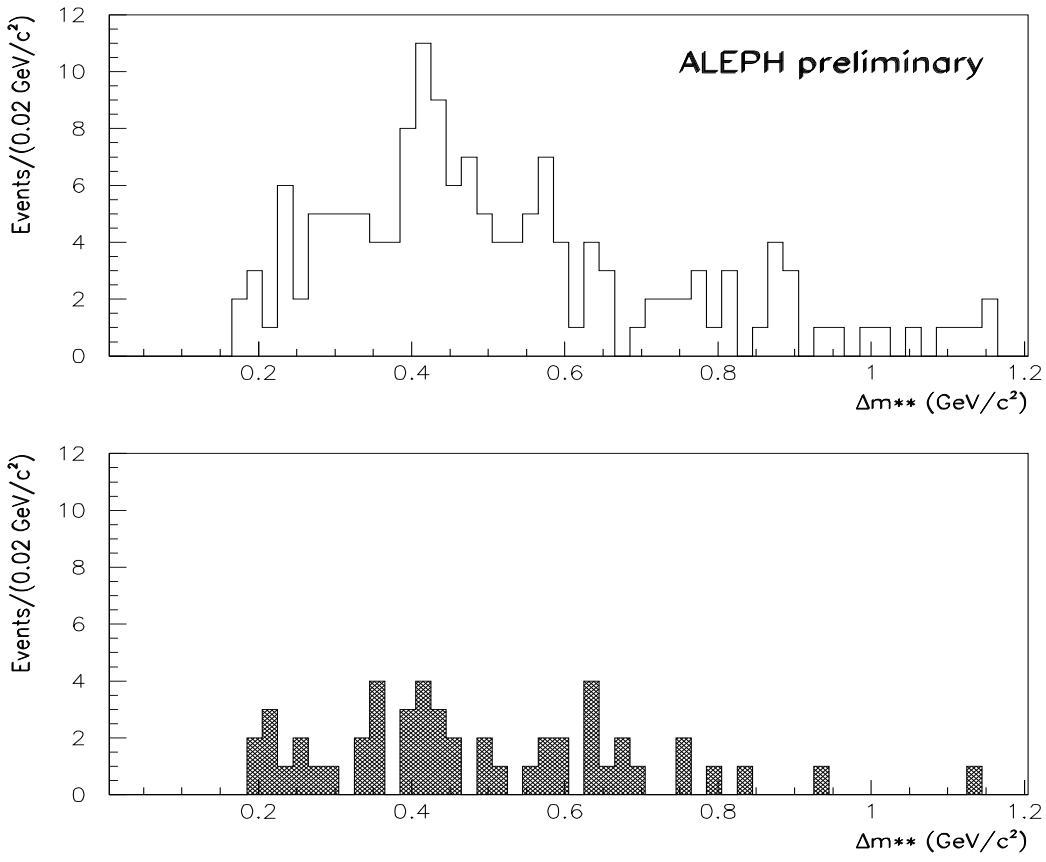

Figure 8: Δm^{**} distribution for right-sign (top) and wrong-sign (bottom) samples for the non-resonant search. Bin width is 20 MeV/c^2.

Source	$D^0\ell$ $\sigma_{syst}(10^{-3})$
Wide vs. non.res. effic.	± 0.38
$\Gamma(Z\to b\overline{b})/\Gamma(Z\to had)$	± 0.06
Background Function	± 0.30
B^0 Vertex Efficiency	± 0.39
Monte Carlo Statistics	± 0.23
D^{*+}, D^0 Branching Ratios	± 0.19
Lepton ID Efficiency	± 0.20
b Fragmentation	± 0.11
B^0 Lifetime	± 0.05
Probability Function $\mathcal{P}$	± 0.12
Total	± 0.74

Table 6: Systematic uncertainties for $D^0\ell$ for the non-resonant search.

4 Conclusions

Evidence for semileptonic B decays into both the D_1^+ resonance and the non-resonant $D^0\pi^+$ (or into wide resonances) is observed by the ALEPH experiment at LEP. The product branching ratio for the D_1^+ production is:

$$\begin{aligned} \mathrm{Br}(b\to\overline{B})\times\mathrm{Br}(\overline{B}\to D_1^+\ell^-\overline{\nu}X)\times\mathrm{Br}(D_1^+\to D^0\pi^+) = \\ = (2.06^{+0.58}_{-0.64}(\mathrm{stat})\,^{+0.30}_{-0.53}(\mathrm{syst}))\times 10^{-3} \end{aligned}$$

From isospin arguments, $\mathrm{Br}(D_1^+\to D^0\pi)$ must be less than 0.66. Using the branching ratio $\mathrm{Br}(b\to B^0)=0.37\pm0.03$ from reference [16], we deduce $\mathrm{Br}(\overline{B}^0\to D_1^+\ell\overline{\nu}X)\geq(8.35\pm3.0)\times10^{-3}$.

At the 95% confidence level,

$$\mathrm{Br}(b\to\overline{B})\times\mathrm{Br}(\overline{B}\to D_2^{*+}\ell^-\overline{\nu}X)\times\mathrm{Br}(D_2^{*+}\to D^0\pi^+)\leq 0.77\times10^{-3}.$$

The product branching ratio for the sum of the decays involving $D^0\pi\ell\nu X$ in the final state is:

$$\mathrm{Br}(b\to\overline{B}^0)\times\mathrm{Br}(\overline{B}\to D^0\pi\ell^-\overline{\nu}X) = (6.46\pm1.57(\mathrm{stat})\pm0.74(\mathrm{syst}))\times10^{-3}.$$

References

[1] Particle Data Group: *Phys. Rev.* **D50** Part I (August 1994).

[2] M. Voloshin and M. Shifman, *Sov. J. Nucl. Phys.* **45** (1987) 292.
M. Voloshin and M. Shifman, *Sov. J. Nucl. Phys.* **47** (1988) 511.
N. Isgur, D. Scora, B. Grinstein, and M. B. Wise, *Phys. Rev.* **D39** (1989) 799.
P. Colangelo, G. Nardulli and N. Paver, *Phys. Lett.* **B293** (1992) 207.

[3] M. Neubert, *Phys. Reports* **245** (1994) 259.

[4] H. Albrecht *et al.*(ARGUS Collaboration), *Phys. Lett.* **B221** (1989) 422.
H. Albrecht *et al.*(ARGUS Collaboration), *Phys. Lett.* **B232** (1989) 398.
J.C. Anjos *et al.*(E691 Collaboration), *Phys. Rev. Lett.* **62** (1989) 1717.
P. Avery *et al.*(CLEO Collaboration), *Phys. Rev.* **D41** (1990) 774.
P.L. Frabetti *et al.*(E687 Collaboration), *Phys. Rev. Lett.* **72** (1994) 324.
P. Avery *et al.*(CLEO II Collaboration), *Phys. Lett.* **B331** (1994) 236.

[5] H. Albrecht *et al.*(ARGUS Collaboration), *Phys. Lett.* **B231** (1989) 208.
P.L. Frabetti *et al.*(E687 Collaboration), *Phys. Rev. Lett.* **72** (1994) 324.
T. Bergfeld *et al.*(CLEO II Collaboration) *Phys. Lett.* **B340** (1994) 194.

[6] H. Albrecht *et al.*(ARGUS Collaboration), *Z. Phys.* **C57** (1993) 533.

[7] R. Akers *et al.*(OPAL Collaboration), CERN-PPE-95-02, submitted to *Z. Phys.*

[8] D. Buskulic *et al.*(ALEPH Collaboration), *Phys. Lett.* **B345** (1994) 103.

[9] D. Decamp *et al.* (ALEPH Collaboration), *Nucl. Instr. Meth.* **A294** (1990) 121.

[10] D. Buskulic *et al.*(ALEPH Collaboration), *Nucl. Instr. Meth.* **A360** (1995) 481.

[11] D. Buskulic *et al.*(ALEPH Collaboration), *Nucl. Instr. Meth.* **A436** (1994) 461.

[12] M. Carpinelli in "Proceedings of the XXVIIth International Conference on High Energy Physics, Glasgow, Scotland" eds. P.J. Bussey and I.G. Knowles (IOP Publ. Ltd., Bristol, 1995)

[13] D. Buskulic *et al.*(ALEPH Collaboration), *Phys. Lett.* **B313** (1993) 535.

[14] P. Avery *et al.*(CLEO II Collaboration), *Phys. Lett.* **B331** (1994) 236.

[15] P.Colas *et al.* in "Proceedings of the XXVIIth International Conference on High Energy Physics, Glasgow, Scotland" eds. P.J. Bussey and I.G. Knowles (IOP Publ. Ltd., Bristol, 1995)

[16] D. Buskulic *et al.*(ALEPH Collaboration), *Phys. Lett.* **B322** (1994) 441.